J. Fluid Mech. (2009), *vol.* 641, *pp.* 169–193.
doi:10.1017/S0022112009991534

Trapping and sedimentation of inertial particles in three-dimensional flows in a cylindrical container with exactly counter-rotating lids

CRISTIAN ESCAURIAZA[1,2] AND FOTIS SOTIROPOULOS[1]†

[1]St. Anthony Falls Laboratory, Department of Civil Engineering, University of Minnesota, Minneapolis, MN 55414, USA

[2]Departamento de Ing. Hidráulica y Ambiental, Pontificia Universidad Católica de Chile, Av. Vicuña Mackenna 4860, 7820436, Santiago, Chile

(Received 16 January 2009; revised 5 August 2009; accepted 6 August 2009; first published online 19 November 2009)

Stirring and sedimentation of solid inertial particles in low-Reynolds-number flows has acquired great relevance in multiple environmental, industrial and microfluidic systems, but few detailed numerical studies have focused on chaotically advected experimentally realizable flows. We carry out one-way coupling simulations to study the dynamics of inertial particles in the steady three-dimensional flow in a cylindrical container with exactly counter-rotating lids, which was recently studied by Lackey & Sotiropoulos (*Phys. Fluids*, vol. 18, 2006, paper no. 053601). We elucidate the rich Lagrangian dynamics of the flow in the vicinity of toroidal invariant regions and show that depending on the Stokes number inertial particles could get trapped for long times in different equilibrium positions inside integrable islands. In the chaotically advected region of the flow the balance between inertia and gravity forces (represented by the settling velocity) can produce a striking fractal sedimentation regime, characterized by a sequence of discrete deposition events of seemingly random number of particles separated by hiatuses of random duration. The resulting staircase-like distribution of the time series of the number of particles in suspension is shown to be a devil's staircase whose fractal dimension is equal to the 0.87 value found in multiple dissipative dynamical systems in nature. Our work sheds new light on the complex mechanisms governing the stirring and deposition of inertial particles and provides new information about the parameters that are relevant in the characterization of particle dynamics in different regions of chaotically advected flows.

Key words: chaotic advection, particle/fluid flows, vortex flows

1. Introduction

Transport and stirring processes in chaotically advected flows (Aref 1984) have been and continue to be the subject of intense research due to their profound role in determining scalar mixing in several engineering and geophysical flows. Recent experimental and computational studies have focused on two- and three-dimensional experimentally realizable flows, yielding new insights into the mechanisms via which flows that are simple from the Eulerian standpoint give rise to chaotic Lagrangian transport and efficient stirring of passive particles (e.g. King *et al.* 2001; Sotiropoulos,

† Email address for correspondence: fotis@umn.edu

Ventikos & Lackey 2001; Sotiropoulos, Webster & Lackey 2002; Solomon & Mezić 2003; Wiggins & Ottino 2004; Lackey & Sotiropoulos 2006). In sharp contrast to the rapidly expanding body of literature dedicated to understanding passive particle dynamics, however, studies with inertial particles in experimentally realizable, chaotically advected flows are rather limited. Yet chaotic advection could play a major role in determining transport and mixing phenomena in a wide range of particle-laden flows in engineering and environmental applications – the separation of particles in dynamic filtration (Wereley, Akonur & Lueptow 2002) and chemical and biological processes in particulate microfluidic systems (Squires & Quake 2005) being just two such examples. Even in geophysical flows dominated by large-scale coherent vortices, chaotic Lagrangian dynamics have been shown to be the primary mechanism for scalar transport and stirring (Ridderinkhof & Zimmerman 1992). It is, thus, reasonable to argue that understanding the Lagrangian dynamics of inertial particles in chaotically advected flows could also contribute to understanding important geophysical problems such as sedimentation processes in natural aquatic environments.

Early studies of inertial particle dynamics focused on idealized two- and three-dimensional analytical flows. Stommel (1949) was the first to study the motion of spherical particles in cellular flows, demonstrating that particles with no inertia in a gravitational field can remain indefinitely suspended depending on the ratio between the fall velocity of the particle and the characteristic velocity of the flow. Maxey (1987) used the same analytical flow to establish that under the influence of gravity all inertial particles heavier than the fluid settle eventually, and their downward trajectories merge in a few selected paths. McLaughlin (1988) computed trajectories of inertial particles in three-dimensional Arnold–Beltrami–Childress (ABC) flows and showed that chaotic advection can be diminished by inertia. He also showed that heavy particles in a gravitational field can remain permanently suspended if they are trapped in periodic orbits in the flow (McLaughlin 1988). Wang, Burton & Stock (1990, 1991) and Wang *et al.* (1992) carried out a complete analysis of inertial particle trajectories in unsteady two-dimensional and ABC flows and estimated the fractal dimension of the phase-space attractor from the Lyapunov exponents of the system, relating their values to some measures of dispersion, such as Taylor's stochastic theory of turbulent diffusion. More recently, Tsega, Michaelides & Eschenazi (2001) studied inertial particles in Hamiltonian two-dimensional unsteady flows using the stream function of Kelvin's cat-eye vortices. They observed chaotic dynamics only for heavy particles with large values of the Stokes number, which is defined as the ratio between the particle response time and the characteristic time scale of the flow (Tsega *et al.* 2001).

Studies of experimentally realizable flows have focused on filtration for dilute suspensions in Taylor–Couette flows between rotating cylinders. Rudman (1998) performed a preliminary analysis of inertial particle stirring in the wavy Taylor–Couette flow. Using the ratio between the velocity scale of the flow and the fall velocity of the particle as a parameter, Rudman (1998) computed how axial dispersion is affected by inertia for slower settling particles and determined that inertial effects produce significant increases in particle dispersion. Wereley & Lueptow (1999) studied the mechanisms that produce particle segregation in rotating filters. Employing an analytical expression for the Taylor vortices and imposing a radial flow, they computed inertial particle trajectories that were very different from the trajectories of fluid particles with the same initial conditions. Wereley & Lueptow (1999) further showed that trajectories of inertial particles approached limit cycles inside the Taylor vortices, trapping them inside toroidal regions for long times, which could explain the efficiency of these filters. A similar experimental analysis of filtration mechanisms by Wereley *et al.* (2002) showed that a combination of the effect of the velocity gradient at the

inner wall with the particle entrainment at the Taylor vortices moves particles away from the filter membrane located at the inner cylinder. These same phenomena were observed in microfluidic devices with dielectric fields (Tuval *et al.* 2005). In these cases, forces induced by electrical fields are used to manipulate the particle dynamics and control their position, producing trapping zones that can separate solid particles in biological suspensions.

In this work we seek to further the understanding of the Lagrangian dynamics of inertial particles in an experimentally realizable steady three-dimensional chaotically advected flow, emphasizing both transport and sedimentation processes. We consider the steady, three-dimensional flow in a closed cylindrical container with exactly counter-rotating lids. The stability of this flow to three-dimensional perturbations has been previously studied by Nore *et al.* (2003, 2004) who showed that there is a range of Reynolds numbers within which the flow becomes three-dimensional but remains steady. The onset of three-dimensionality is the result of a Kelvin–Helmholtz-type instability of the azimuthal shear layer that gives rise to the growth of radial vortices. The fact that the flow in this axisymmetric geometry with simple boundary conditions transitions to a complex, three-dimensional state but remains steady over a reasonably broad range of Reynolds numbers makes it an excellent test case for investigating chaotic advection in a steady experimentally realizable flow. Lackey & Sotiropoulos (2006) studied numerically the dynamics of passive Lagrangian tracers in this flow for Reynolds numbers in the three-dimensional, steady regime. They showed that the rate at which passive tracers are stirred by the chaotically advected flow is not a monotonic function of the Reynolds number. Rather an optimal Reynolds number exists at which the stirring rate is maximized. For higher Reynolds number the stirring rate was shown to decrease at a rate consistent with the theory developed by Mezić (2001). In this paper we report a systematic, one-way coupling numerical investigation of transport, stirring and sedimentation processes of small inertial particles in a flow in the container with exactly counter-rotating lids, using the steady, three-dimensional velocity fields obtained numerically by Lackey & Sotiropoulos (2006). We seek to explore questions regarding the persistence of unmixed islands and chaotic regions in the flow and identify sedimentation mechanisms as various governing parameters, such as the particle Stokes number and settling velocity, are varied systematically. The range of parameters is selected to perform simulations in realistic particle flows, such that the model can be also used to design experiments and study general stirring problems of inertial particles in chaotic advection. Our results yield novel insights into the complex relationship between the various forces and the particle dynamics and show that there is a range of governing particle parameters within which a striking fractal sedimentation regime emerges.

The paper is organized as follows. A brief description of the flow used as the test bed in this paper and a summary of previous work on this flow are provided in § 2. The governing equations of the particle model are explained in § 3. In § 4 we show the main characteristics of the particle dynamics in invariant regions and the effects of inertia on the trapping inside the tori that exist for all the Reynolds numbers studied. In § 5 we explore the mixing region, focusing on deposition and activation of a fractal sedimentation regime represented by the devil's staircase. The conclusions in § 6 contain the implications of this study and summarize future ideas for research.

2. Flow in a container with exactly counter-rotating lids

We consider laminar flow of incompressible Newtonian fluid of kinematic viscosity ν, in a closed cylinder of height H and radius R (see figure 1 for a schematic of the

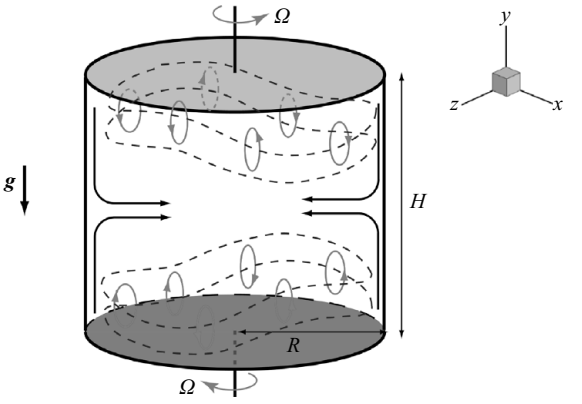

FIGURE 1. Schematic topology of the flow in a container with exactly counter-rotating lids showing the invariant toroidal regions. The arrows mark the direction of the flow at the central plane of the container that rotates in opposite directions and generates a shear layer. The acceleration of gravity is parallel to the cylinder axis.

flow and definitions). The flow is driven by the top and bottom lids, which rotate in opposite directions at the same constant angular velocity Ω, and is governed by two non-dimensional parameters: the Reynolds number based on the cylinder radius,

$$Re = \frac{\Omega R^2}{\nu}, \tag{2.1}$$

and the aspect ratio of the container,

$$AR = H/R. \tag{2.2}$$

As in Lackey & Sotiropoulos (2006) we consider the case $AR = 1$ for which numerical simulations have shown that the flow remains steady and axisymmetric for $Re < 300$. At higher Reynolds numbers the flow becomes three-dimensional but remains steady over a relatively wide range of Reynolds numbers – Lackey & Sotiropoulos (2006) reported steady three-dimensional solutions for Reynolds numbers as high as $Re = 850$. The onset of three-dimensionality in the flow is characterized by the growth of the $m = 3$ azimuthal mode in the form of radial cat-eye vortices at the equatorial plane. The instability is essentially the radial equivalent of the Kelvin–Helmholtz instability in linear shear layers and gives rise to a very complex steady three-dimensional flow consisting of radial and axial inclined vortices. The calculated flow fields of Lackey & Sotiropoulos (2006) were shown to be in good agreement with previous stability analyses for this flow by Nore *et al.* (2003, 2004) and were employed to study the chaotic dynamics of Lagrangian transport of passive tracers over the entire range of simulated Reynolds numbers, $300 < Re < 850$. A major new finding reported in Lackey & Sotiropoulos (2006) is that the stirring rate in this flow is not a monotonic function of the Reynolds number. The stirring rate was shown to initially increase for $300 < Re < 500$ but to attain a maximum at $Re \approx 500$. Further increase in the Reynolds number was shown to cause the stirring rate to decrease monotonically at a rate proportional to $Re^{-1/2}$. The decline in stirring efficiency was shown to be due to the growth with the Reynolds number of the regions in the flow occupied by unmixed islands. This striking finding is explained by and appears to support a recently proposed theory of chaotic advection (Mezić 2001). According to the theory, in steady confined three-dimensional chaotically advected flows the

mixing rate should eventually decrease with increasing Reynolds number at a rate proportional to the thickness of the near-wall boundary layer ($\sim Re^{-1/2}$).

In what follows, we employ the numerically simulated flow fields obtained by Lackey & Sotiropoulos (2006) to carry out such an investigation. All velocity fields analysed in this paper have been obtained on a polar cylindrical grid with $81 \times 211 \times 161$ nodes in the radial, axial and azimuthal directions, respectively. This grid was shown by Lackey & Sotiropoulos (2006) to be adequate for obtaining grid-independent solutions. The reader is referred to the paper of Lackey & Sotiropoulos (2006) for more details on the numerical method and other computational details.

3. Computational model of inertial particles

3.1. *Particle equations and governing parameters*

We simulate the motion of inertial particles in the steady flow fields, assuming one-way coupling; that is the concentration of particles is sufficiently small not to affect the flow of the carrier fluid. The governing equations are the particle trajectory and momentum equations, which read in tensor form as follows ($i = 1, 2, 3$):

$$\frac{\mathrm{d}x_i}{\mathrm{d}t} = v_i, \tag{3.1}$$

$$m\frac{\mathrm{d}v_i}{\mathrm{d}t} = f_i. \tag{3.2}$$

In the above equations, v_i and x_i are the ith component of the particle velocity and position vectors, respectively; m is the particle mass; and f_i represents the ith component of the total force acting on the particle.

In the most general case, the total force contains contributions from drag, gravity, lift, added mass and pressure and viscous forces. Calculating these forces using analytical expressions obtained for spherical non-rotating particles, a general momentum equation can be written as follows (Crowe, Troutt & Chung 1998):

$$m\frac{\mathrm{d}\boldsymbol{v}}{\mathrm{d}t} = \frac{1}{2}\rho C_D \frac{\pi\tilde{d}^2}{4}|\boldsymbol{v}_r|\,\boldsymbol{v}_r + \left(1 - \frac{\rho}{\rho_s}\right) m\boldsymbol{g} + \rho C_L \frac{\pi\tilde{d}^3}{6}(\boldsymbol{v}_r \times \boldsymbol{\omega}) + \rho C_m \frac{\pi\tilde{d}^3}{6}\left(\frac{\mathrm{D}\boldsymbol{u}}{\mathrm{D}t} - \frac{\mathrm{d}\boldsymbol{v}}{\mathrm{d}t}\right) + \rho\frac{\pi\tilde{d}^3}{6}(-\nabla p + \mu\nabla^2\boldsymbol{u}), \tag{3.3}$$

where $\boldsymbol{u}$ and $\boldsymbol{v}$ are the fluid and particle velocity vectors, respectively; $\boldsymbol{v}_r = (\boldsymbol{u} - \boldsymbol{v})$ is the relative velocity; ρ is the density of the fluid; and ρ_s is the density of the particles. The first term on the right-hand side of (3.3) is the drag force. The drag coefficient C_D is a function of the particle Reynolds number, which for particles of diameter $\tilde{d}$ is defined as follows:

$$Re_r = \frac{|\boldsymbol{v}_r|\,\tilde{d}}{\nu}. \tag{3.4}$$

Extensive numerical tests, in which we compared the values of C_D and particle trajectories with the same initial conditions for different expressions of the drag coefficient (Crowe *et al.* 1998), showed that Stokes drag is a good approximation for determining C_D. Therefore, the drag coefficient in (3.3) is computed as follows (Crowe *et al.* 1998):

$$C_D = \frac{24}{Re_r}. \tag{3.5}$$

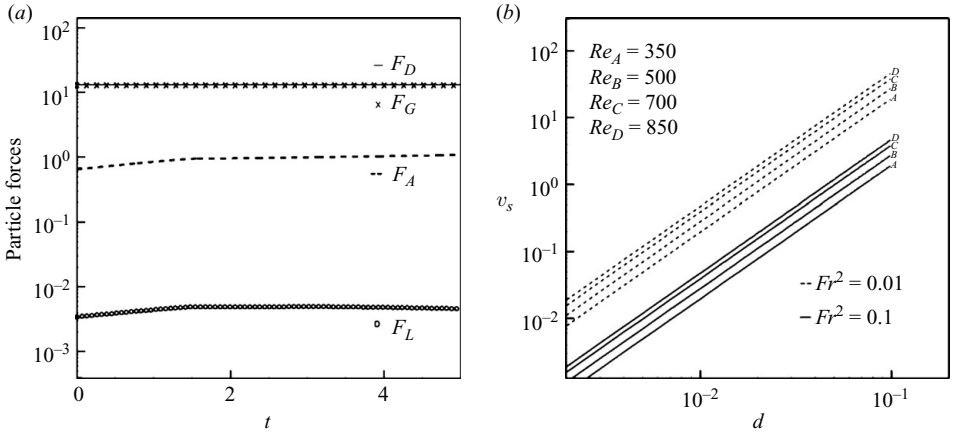

FIGURE 2. (*a*) Magnitude of particle forces during a simulation; lift F_L and added mass with pressure and viscous stresses F_A are at least one order of magnitude smaller than drag F_D and gravity F_G. (*b*) Settling or terminal velocity v_s, as a function of non-dimensional particle diameter for two different Froude numbers.

The second force term on the right-hand side of (3.3) is the gravitational force. The acceleration of gravity is assumed to act vertically downward along the negative x_3 axis, such that $g_i = -g\,\delta_{i3}$, where g is the gravitational constant and δ_{ij} is Kronecker's delta.

The remaining forces in (3.3) correspond to the lift force, added mass and fluid stresses. The lift mechanism considers the velocity gradient around a particle moving in a non-uniform rotational flow. The lift coefficient C_L has been considered constant for inviscid flows (Auton, Hunt & Prud'homme 1988) or expressed as a function of the vorticity magnitude and the particle Reynolds number in the Stokes regime (Saffman 1965). The added mass coefficient is in general considered constant, equal to the inviscid approximation, $C_m = 0.5$ (Crowe *et al.* 1998). The last two terms in (3.3) are forces induced by flow stresses and can be calculated by interpolating the flow field variables at the current particle position.

Including all these forces in the particle momentum equation (3.2) is neither efficient nor necessary, as the relative magnitude of some of them is essentially negligible compared to others. To explore the relative magnitude of the various forces in the present flow we carried out systematic numerical experiments in order to identify which of the forces make a significant contribution to the particle momentum budget. Our numerical experiments showed that the lift and added mass forces and the forces due to flow-induced stresses are smaller by at least one order of magnitude compared to the drag force, as shown in figure 2(*a*). Based on these numerical findings and for the sake of computational expedience we simplified the particle momentum equation (3.3) by retaining on its right-hand side only the drag and gravity forces. After non-dimensionalizing, respectively using R and ΩR as the length and velocity scales, the final form of the particle momentum equation we use in all our subsequent simulations reads as follows:

$$\frac{\mathrm{d}v_i}{\mathrm{d}t} = \frac{1}{SG}\left(\frac{1}{St}v_{ri} - \frac{\delta_{i3}}{Fr^2}\right), \tag{3.6}$$

where v_i is now the non-dimensional particle velocity and v_{ri} represents the non-dimensional relative particle velocity, defined as the difference between the local flow

and particle velocities, $v_{ri} = u_i - v_i$. The three dimensionless parameters in the above equations are defined as follows: SG is the ratio of the particle density to the fluid density, i.e. the particle specific gravity $SG = \rho_s/\rho$. In our simulations, SG is set to be constant and equal to the common value associated with sand grains in water ($SG = 2.65$).

The Froude number Fr is the ratio of inertia and modified gravity and is defined as

$$Fr = \frac{\Omega R}{\sqrt{(SG-1)gR}}. \tag{3.7}$$

Finally the Stokes number St is defined as the ratio of the particle relaxation time to the characteristic time scale of the flow in the container and serves to identify the dynamical relation between the two phases. Since the drag is the dominant force, the Stokes number is defined as

$$St = \frac{4}{3}\frac{d}{C_D\,|\boldsymbol{v}_r|} = \frac{d^2}{18}Re. \tag{3.8}$$

where $d = \tilde{d}/R$ corresponds to the non-dimensionalized particle diameter. The Stokes number quantifies the influence of the flow on the particles (Crowe *et al.* 1998). For the computations performed in this study $St \ll 1$, and thus particles have enough time to respond to changes in flow velocity along their trajectories.

The expression given by (3.8) shows that for a given Reynolds number the Stokes number depends only on the non-dimensional particle diameter. Thus, for each Re the magnitude of the inertial term on the right-hand side of (3.6), i.e. the expression for the drag force that depends solely on St, is set by choosing a non-dimensional particle diameter. The magnitude of the gravitational term, on the other hand, is established by selecting the Froude number. This approach can be thought of as implicitly modifying either the relation between Ω and R or the fluid viscosity.

A perfectly elastic collision scheme is also implemented in the model to account for the interaction with the boundaries. The model, however, does not consider inter-particle collisions or the influence of the inertial particles on the flow. Upon impact, only the normal component of the particle velocity with respect to the boundary is modified according to the following relation:

$$v_{\hat{n}} = -v_{\hat{n}}, \tag{3.9}$$

where $v_{\hat{n}}$ is the projection of the particle velocity on to the direction normal to the solid surface, i.e. $v_{\hat{n}} = v_i\,\hat{n}_i$. Further details of the particle model can be found in Escauriaza (2008).

A relevant parameter to classify the particle dynamics and quantify the results of the simulations is the magnitude of the particle settling or terminal velocity v_s, which can be obtained by combining St and Fr into a single parameter as follows (Rudman 1998; Dávila & Hunt 2001):

$$v_s = \frac{St}{Fr^2}. \tag{3.10}$$

This is the same parameter derived by Maxey (1987) and Rudman (1998) in the simulations of inertial particle dynamics and one of the dimensionless quantities utilized recently by Dávila & Hunt (2001) in the study of small particle trajectories near vortices. Figure 2(*b*) shows the relation between v_s and the particle diameter for $Fr^2 = 0.01$ and 0.001 and various Reynolds numbers. Using the expressions in (3.7), (3.8) and (3.10), we observe that smaller Fr^2 or larger diameter results in

higher gravitational forces and higher settling velocities. The subsequently reported simulations were performed for different combinations of d and Fr^2, resulting in a broad range of settling velocities $1 \times 10^{-6} \leqslant v_s \leqslant 0.1$. The flow fields we employ were obtained for $Re = 350$, 500, 700 and 850 (Lackey & Sotiropoulos 2006).

3.2. *Numerical integration details*

The first step in the numerical integration of the particle momentum equation (3.6) is to calculate the terms on its right-hand side at the current particle location. This is accomplished by interpolating the flow variables from the surrounding Eulerian grid nodes to the particle's position using the second-order tri-linear interpolation procedure explained in Sotiropoulos *et al.* (2001). Following this step, the momentum and trajectory equations, (3.6) and (3.1), are advanced in time using a fourth-order Runge–Kutta scheme (as in Sotiropoulos *et al.* 2001), employing a non-dimensional time step of 10^{-5} of a lid rotation.

The particle tracking and numerical solution methods were validated using the numerical simulations performed by McLaughlin (1988) in ABC flows as benchmark. The analytical ABC solution was assigned to a three-dimensional grid with 10^6 nodes, and the trajectory and momentum of inertial particles were computed by interpolating the flow variables to the location of the particles, instead of obtaining these quantities directly from the analytical ABC velocity equations. The results reproduced all the trajectories of inertial particles simulated by McLaughlin (1988) with excellent accuracy, including the capturing of heavy particles in periodic orbits. The details of the numerical method along with the results of the validation study can be found in Escauriaza (2008).

4. Particle trapping in invariant regions

Lackey & Sotiropoulos (2006) showed that for the entire range of simulated Reynolds numbers for which the flow is three-dimensional ($Re > 300$), the dynamics of passive particle transport is very rich and is characterized by topologically complex, toroidal invariant regions embedded in the chaotic sea that occupies most of the container (see figure 14 in Lackey & Sotiropoulos 2006). In this section we seek to explore the existence and persistence of invariant regions for inertial particles over a range of particle governing parameters. The results shown in this section have been obtained using the velocity field for $Re = 350$. Similar results, however, have been obtained for all simulated Reynolds numbers.

The particle dynamics in the flow can be observed by plotting Poincaré sections at vertical ($\theta = \text{const.}$) planes across the cylinder. We constructed such return maps for the entire range of simulated settling velocities ($1 \times 10^{-6} \leqslant v_s \leqslant 0.1$) by placing 10^4 particles in the chaotic region of the flow and tracking their trajectories for 50 lid rotations. A typical Poincaré section is shown in figure 3(a) for $v_s = 1 \times 10^{-5}$. The simulated trajectories clearly show that toroidal barriers to transport similar to those observed by Lackey & Sotiropoulos (2006) for passive particles are also present for inertial particles. It is evident from this figure that the interior of these toroidal regions is not accessible to particles originating in the chaotic region, at least within the simulated time interval. Even though not shown herein due to space considerations, similar unmixed toroidal regions are found for all simulated settling velocities. On the other hand, particles that originate in the interior of the invariant regions depicted in figure 3(a) are found to remain trapped for very long times, but their trajectories can be markedly different depending on the particle governing parameters. This is shown

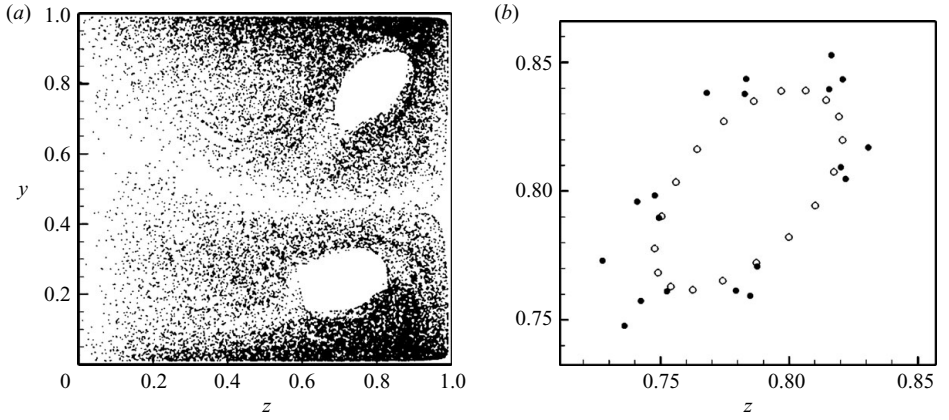

FIGURE 3. Poincaré maps of inertial particles with settling velocity $v_s = 1 \times 10^{-5}$ and $Re = 350$, at $X = 0$. (*a*) Poincaré section for 10 000 particles with $d = 0.002$. (*b*) Poincaré section of two particles trapped in the upper torus with different diameters and the same settling velocity, $d = 0.002$ (○) and $d = 0.007$ (●).

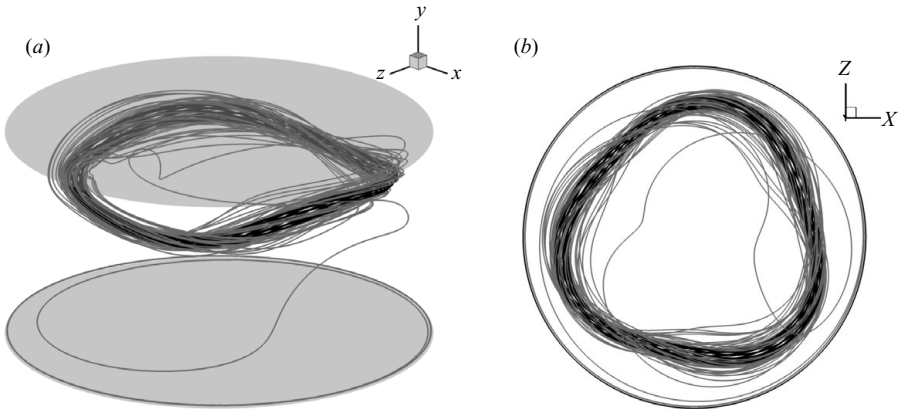

FIGURE 4. Trajectories of particles with different values of *St* inside the upper torus for $Re = 350$. The small particle with $d = 0.002$ remains trapped (black line), while the larger particle with $d = 0.007$ (grey line) escapes and sediments after 163 lid rotations. For both cases $Fr^2 = 0.02$.

in figure 3(*b*), which shows a Poincaré section for two particles with identical v_s but different *St* (established by varying the particle diameter), starting from exactly the same initial position within the upper invariant toroidal region shown in figure 3(*a*). Note that maintaining the same terminal velocity for two particles with different Stokes numbers requires changing the gravitational force, i.e. the Froude number. As seen in figure 3(*b*), the dynamics of the particles for the range of parameters selected depends strongly on the particle Stokes number. As depicted in figure 4, the small-*St* ($d = 0.002$) particle behaves, as one would anticipate, essentially like a passive tracer, and its trajectory remains confined during the entire simulation period of 200 lid rotations on a torus forming a limit cycle in the Poincaré section. The larger *St* ($d = 0.007$) particle, on the other hand, is seen to gradually spiral around the outer part of the torus with changing return periods and eventually escapes after 163 lid rotations.

The results shown in figures 3 and 4 as well as those we have obtained for other values of St point to the important conclusion that even though the invariant toroidal regions of the flow (as seen in the transport of passive particles) do exist for inertial particles as well, particle inertia will ultimately cause particles to escape from the invariant regions and explore the rest of the flow domain or settle towards the bottom lid as we will see in the following section. The effect of particle inertia is obviously quantified by St, which appears to dictate the residence time of particles in the interior of invariant regions. In the limit as $St \to 0$ particles will behave as passive, non-diffusive tracers and will remain trapped on KAM surfaces indefinitely. On the other hand, for $St > 0$ particles will eventually escape due to the effects of inertia, but the time they will remain trapped in invariant regions of the flow is a decreasing function of their Stokes number. Clearly our results suggest that the capacity of the flow to trap inertial particles in invariant toroidal regions should also depend on the magnitude of the Stokes number and not only on the value of the settling velocity v_s. It is worth emphasizing here that all these results are applicable to the range of parameters studied, which also consider a constant specific gravity of the inertial particles.

The particle trapping mechanisms discussed above were also observed by Wereley & Lueptow (1999) and Wereley *et al.* (2002) in rotating filters. The efficiency of these filters is directly related to the capacity of the Taylor vortices and the azimuthal velocity gradient to capture and trap inertial particles. The fact that trapping zones coincide with invariant regions of the fluid flow has also been observed in the experiments of Abatan, McCarthy & Vargas (2006) for the flow in a cylindrical tank with co-rotating flat-disk impellers. Abatan *et al.* (2006) showed that particles are displaced inside the toroidal regions after long periods of time, reaching different equilibrium positions either inward or outward towards the torus surface.

To gain a more complete understanding of the richness of dynamics near invariant regions, we utilize the Lagrangian averaging technique proposed by Mezić & Wiggins (1999). Lagrangian averaging is a very effective computational technique for visualizing invariant regions in chaotically advected flows and has also been used to develop a non-intrusive experimental method for visualizing unmixed islands in chaotically advected flows (Mezić & Sotiropoulos 2002; Sotiropoulos *et al.* 2002). Assuming steady three-dimensional flow, the Lagrangian averaging technique can be implemented as follows. Associate with any point A of the flow field the Lagrangian time average of a function f (some property of the flow field) along the particle trajectory that passes through A. This quantity can be computed by averaging over the values of f at the points visited by the particle as it moves along its trajectory (Malhotra, Mezić & Wiggins 1998; Mezić & Wiggins 1999). The fact that as time approaches infinity such an average exists can be rigorously established from ergodic theory (Mezić & Sotiropoulos 2002). The invariant regions of the Poincaré map of the flow can then be visualized by (i) distributing a sufficiently large number of initial points on a plane through the flow field, (ii) computing the Lagrangian time averages of the chosen function f for all these points and (iii) plotting the isocontours of the resulting scalar field in terms of the initial particle locations. It can be shown (Malhotra *et al.* 1998; Mezić & Wiggins 1999) that regular islands in the flow are found around the extrema of the Lagrangian time-averaged field. Lagrangian averaging has already been used by Lackey & Sotiropoulos (2006) to visualize invariant regions in the present flow over a range for Reynolds numbers. Here we utilize Lagrangian averaging to visualize the rich dynamics of inertial particles near invariant tori over a range of particle motion governing parameters.

We construct Lagrangian average maps by defining a set of 100×100 initial conditions uniformly distributed on a $\theta = \text{const.}$ plane and compute averages of the particle velocity magnitude along particle trajectories employing the same methodology described in detail by Lackey & Sotiropoulos (2006). The Lagrangian-averaged particle velocity magnitude U_{ij}^L is defined as follows:

$$U_{ij}^L = \frac{\bar{u}_{ij}^L - \langle u \rangle}{\langle u \rangle}, \tag{4.1}$$

where $\bar{u}_{ij}^L$ is the particle velocity magnitude (which is equal to the local flow velocity for passive particles) averaged along the particle trajectory originated at the (i, j) position and $\langle u \rangle$ is the Eulerian average velocity magnitude over the entire container. A qualitative explanation why invariant regions will be located in the vicinity of maxima of U^L in the Lagrangian average map is as follows. If most of the flow is occupied by chaotic trajectories and the (i, j) particle originates in the chaotic region, U_{ij}^L will be close to zero. This is because such a particle would cover ergodically the entire chaotically advected region of the flow, and thus the Lagrangian average of the velocity magnitude would be very close to its Eulerian average over the entire container. On the other hand, if a particle is placed in an invariant region and as such can only sample a small portion of the flow domain, U_{ij}^L will acquire a large magnitude. It is important to emphasize, however, that the above arguments as well as the theory presented in Mezić & Wiggins (1999) are strictly valid for passive particles. As we will show below, in the case of inertial particles U^L can acquire very large values even for particles that originate within chaotic regions. This is because such particles will, under the action of gravity, settle eventually to the bottom rotating lid. Since in our model particles that sediment do not get resuspended by the flow but rather stay at the bottom and move forever with the velocity of the rotating lid, U_{ij}^L for these points attains the maximum possible magnitude in the flow domain. This issue not withstanding, however, Lagrangian average maps can provide important qualitative information about the rich dynamics of inertial particle transport, and in particular they should be able to readily identify invariant regions in which particles are trapped for very long times. Such regions for inertial particles will be characterized by a smoothly varying U^L field and contour levels distinctly different from, although not necessarily larger than, those in the surrounding chaotic sea.

As a base for comparison we start by discussing the Lagrangian average map for passive particles shown in figure 5(*a*). We can readily distinguish in this map the toroidal invariant core of the flow where U^L varies smoothly and attains large values. The invariant core is surrounded by the chaotic sea which is characterized by a very distinct fractal-like distribution of U^L contours. Note in particular the Cantor-dust-like set of points that are distributed throughout the darker-colour chaotic sea in which U^L attains very large magnitude, pointing to the existence of a Cantor set of very high-order invariant orbits. What is even more striking in this plot is the structure of the contours near the interface between the invariant core of the flow and the chaotic sea. Even though it is evident from this figure that the invariant core creates an impermeable barrier to transport, the transition zone between the integrable core and the chaotic region in this map as well as in the results of Lackey & Sotiropoulos (2006) is not smooth and is occupied by a series of islands that contain periodic orbits intermingled with chaotic areas. To elucidate the dynamics in this transition zone, we show in figure 5(*b*) a Lagrangian average map constructed by embedding all 10^4 initial conditions within a small patch of the larger map shown in figure 5(*a*). As seen

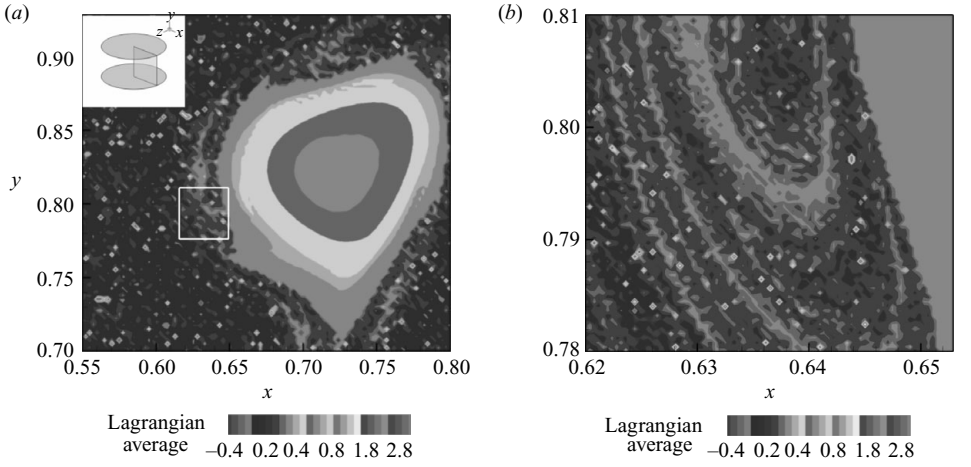

FIGURE 5. (*a*), (*b*) Lagrangian average maps with increasing resolution for $Re = 350$, showing the upper toroidal invariant region, and narrow bands of periodic orbits nested and folded near the boundary of the torus.

in figure 5(*b*), the dynamics in the transition zone is very rich and is characterized by the existence of nested structures that appear as foldings of integrable dynamics, with narrow bands that seem to have a fractal distribution in space. By examining the trajectories of passive particles starting from these regions (not shown herein) we observe that inside the folded islands particles have distinctly different dynamics, spiralling quasi-periodically around the toroidal invariant core without completing closed loops and remaining always near the boundary of the integrable core with their motion restricted to regions of the map inside the integrable folds (typical three-dimensional trajectories showing this structure of the tori can be observed in figure 14 of Lackey & Sotiropoulos 2006). Similar results were found for passive particles at all the different Reynolds numbers, with maps that also show thin bands of periodic trajectories distributed in the outer region of the invariant tori. It is important to note that these folded islands are not cantori, i.e. leaky barriers to transport (Mackay, Meiss & Percival 1984), as passive non-diffusive particles will remain trapped within these structures of enormous topological richness for ever.

To systematically gauge the effects of inertia and gravity on particle dynamics, we construct Lagrangian average maps for different particle diameters and Froude numbers using the same set of 10^4 initial conditions as those used in figure 5. For small values of St and large Fr, the Lagrangian maps of inertial particles show a fairly uniform velocity along the periodic orbits inside the invariant regions. For the simulations with $d = 0.002$ and $Fr^2 = 0.2$ depicted in figure 6(*a*), the map shows smaller velocities for the inertial particles compared to the Lagrangian average maps for the passive tracers (see figure 5). The higher-resolution map shown in figure 6(*b*), reveals characteristics similar to those of the Lagrangian average maps for passive particles, with numerous bands of periodic orbits distributed as nested folds in selected areas near the boundary of the torus. To increase the relative importance of the gravitational force while keeping the particle diameter constant we decrease Fr^2 by one order of magnitude, and the resulting Lagrangian maps are shown in figures 6(*c*) and 6(*d*) ($d = 0.002$ and $Fr^2 = 0.02$). It is seen that for sufficiently large gravitational force, the chaotic flow outside the invariant regions is no longer capable of maintaining

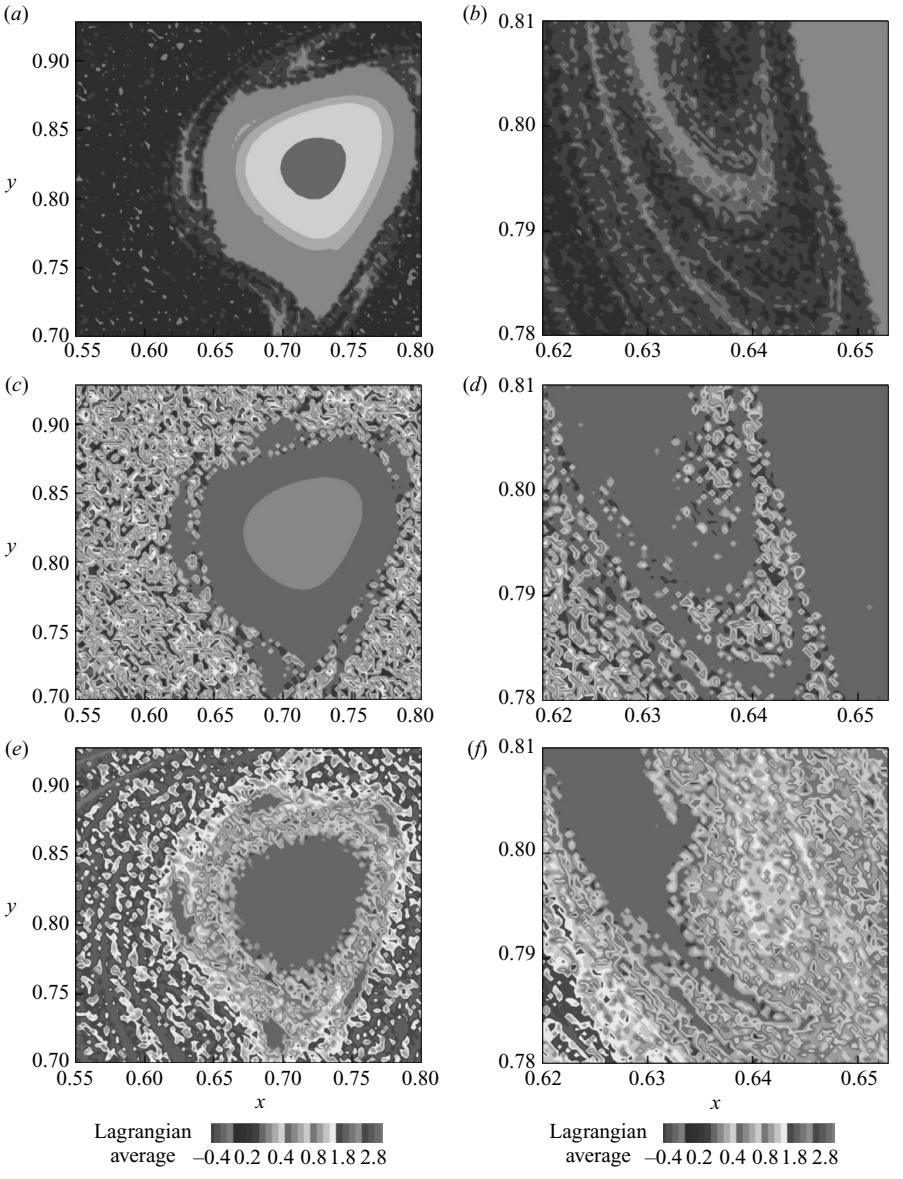

FIGURE 6. Maps for inertial particles contain the average velocity magnitudes of inertial particles, scaled with the average flow velocity inside the container for 50 lid rotations. (*a*), (*b*) The particle diameter and Froude number are $d = 0.002$ and $Fr^2 = 0.2$ respectively. (*c*), (*d*) The results for $d = 0.002$, and a larger gravitational term with $Fr^2 = 0.02$. (*e*), (*f*) With larger Stokes number given by $d = 0.006$ and $Fr^2 = 0.2$.

the particles in suspension. This is evident by the fact that the average values in the fractalized chaotic zone become very large, since, as already discussed above, most of the particles originating in this region sediment quickly and end up on the bottom lid of the container. A striking finding seen in figure 6(*c*), however, is that even though the perturbation introduced on the inertial particles by the relatively strong gravitational force is considerable, the size of the invariant toroidal region does not change in

any appreciable manner. Particles continue to remain trapped inside the toroidal core or within the topologically rich integrable islands formed within the transition zone. From the magnified map shown in figure 6(*d*), we can readily identify that the complex islands around the torus become coarser, and particles trapped in their interior have overall smaller average velocities. Finally, figures 6(*e*) and 6(*f*) show Lagrangian maps for larger Stokes number and the same value of *Fr* as that shown in figures 6(*a*) and 6(*b*). It is seen that increasing *St* while keeping *Fr* constant causes the total area of the invariant core to decrease considerably. Particles near the boundary of the original torus escape to the chaotic region within the total time of the simulation, forming the irregular lighter-colour area at the border of the invariant region depicted in the Lagrangian average map of figures 6(*d*) and 6(*e*). In addition, the folded structures start to become high-period islands with a defined boundary, where quasi-periodic trajectories are maintained as equilibrium position of these initial conditions.

In summary, the key conclusion from the results presented in this section is that regions in the flow that are impermeable barriers to transport for passive tracers persist for inertial particles as well. The key governing parameter that determines the ability of an invariant flow region to trap inertial particles for very long times is the particle *St*, since the drag generated by the relatively uniform velocity fields seen by particles originating in invariant regions is capable of keeping inertial particles trapped. Contrary to what one might have anticipated, the magnitude of *Fr*, and by extension the relative magnitude of the gravity force, has little influence on whether particles will escape an invariant region or remain trapped for arbitrarily long times. The Froude number of course, or equivalently the settling velocity, does determine how quickly particles in the mixed region of the flow will sediment at the bottom of the container.

5. Particle deposition: settling down the devil's staircase

Material lines originating in chaotic regions undergo continuous stretching and folding by the chaotically advected flow, leading to exponential separation of initial conditions and efficient stirring. Lackey & Sotiropoulos (2006) investigated the chaotic stirring of passive tracers by the flow under consideration across a wide range of Reynolds numbers. To demonstrate the process of chaotic stirring for inertial particles, we show in figure 7 instantaneous snapshots illustrating the stirring of three spherical blobs of identical diameter equal to 0.1, each consisting of 1000 identical initial conditions. One blob, however, consists of passive (grey) particles, while the other two blobs contain inertial particles with $d = 0.007$ and $v_s = 1 \times 10^{-5}$ (white) and $v_s = 1 \times 10^{-3}$ (black), respectively (i.e. same *St* but different *Fr*). The results illustrate that initially all three blobs undergo similar stretching and folding processes as they are advected by the flow within the container. Up until four lid rotations the three blobs have spread in a similar manner with the heaviest (black) particles showing a clear tendency to diverge from the other two sets of particles. After 10 more lid rotations any initial structure has been lost, as the repeated stretching and folding processes have led to exponential separation and caused the random dispersion of particles within the entire domain. An interesting feature that is evident in figure 7(*c*), however, is that after 14 lid rotations most of the heavier black particles have settled on the bottom lid and have been pushed away to the corner by the centrifugal force.

The fact that under the action of gravity particles will eventually sediment at the bottom of the container is obviously not surprising. The results shown is figure 7, however, do raise an important question regarding the rate at which particles of different properties will settle under the action of gravity. For the inertial particles

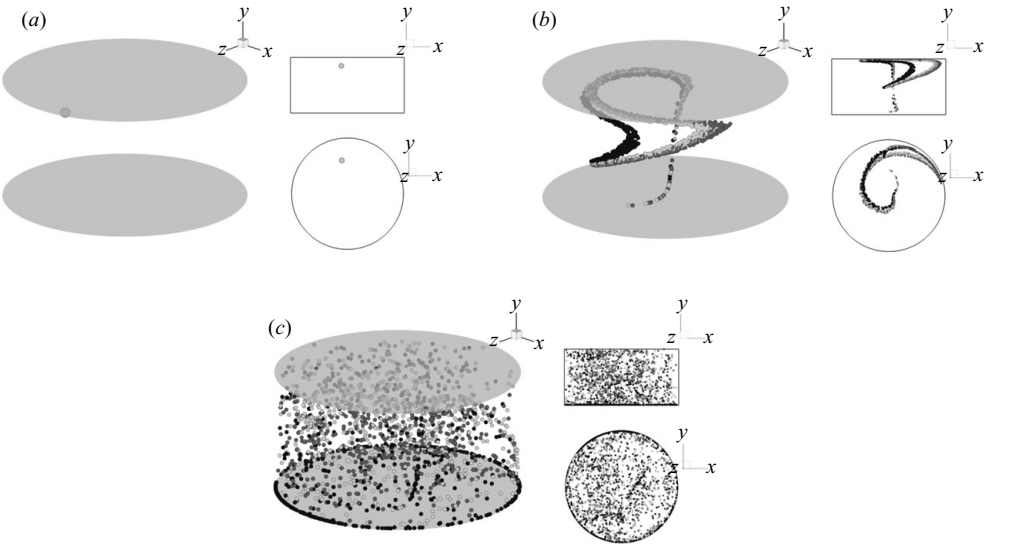

FIGURE 7. Three thousand particles in the chaotically advected region at $Re = 350$. Grey particles are passive, while white and black have $v_s = 1 \times 10^{-5}$ and $v_s = 1 \times 10^{-3}$, respectively, and $d = 0.007$: (*a*) initial conditions, (*b*) after four lid rotations and (*c*) after 14 lid rotations.

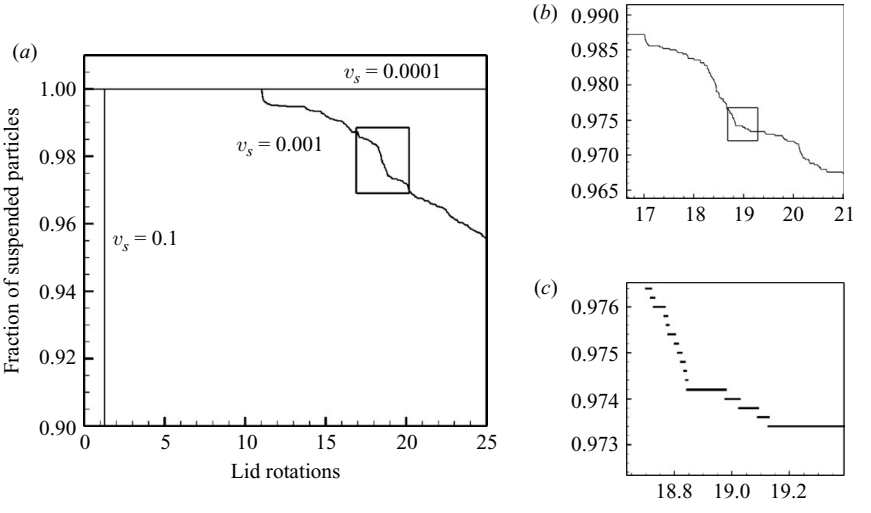

FIGURE 8. Fraction of suspended particles for $d = 0.006$ and $Re = 500$. (*a*) Curves for different settling velocities. (*b*), (*c*) Magnification of the fractal curve in the rectangular regions for $v_s = 0.001$, showing the self-similar structure of the devil's staircase.

in figure 7, gravity introduces a drift in the vertical direction that depends on the magnitude of the Stokes number relative to the Froude number, which is quantified by the settling velocity given by (3.10). As $v_s \to \infty$, the inertial effects cannot maintain suspension, and rapid sedimentation will abruptly terminate the stirring process. On the other hand, in the limit $v_s \to 0$ particles behave as passive tracers, and in the absence of molecular diffusion stirring will continue indefinitely. The question that we would like to explore herein is exactly how the transition between these two limiting states takes place as the settling velocity varies from zero to infinity.

To explore the rate of particle deposition as a function of the settling velocity, we plot in figure 8(*a*) the temporal variation of the fraction of an initial population of particles that remain in suspension at a given instant in time. The results shown in figure 8 have been obtained by releasing 5000 particles along a series of concentric circles covering the entire top lid for $Re = 500$. We consider three types of particles, all having the same diameter d (i.e. fixed Stokes number) but with settling velocities varying across three orders of magnitude: $v_s = 10^{-1}, 10^{-3}$ and 10^{-4}. As we already discussed in the previous paragraph, for $v_s = 10^{-4}$ the inertial particles are dispersed throughout the entire container; the stirring process continues for very long times; and the rate of particle deposition is sluggish. On the other hand, for the largest settling velocity ($v_s = 10^{-1}$) shown in figure 8(*a*) gravity dominates the particle dynamics and the sedimentation process is monotonic and rapid with all particles depositing on the bottom lid within a few lid rotations.

A striking new finding that follows from figure 8(*a*) is the sedimentation regime that emerges for settling velocities in the transitional state between the two limiting cases. As seen in figure 8(*a*), the particle deposition process for $v_s = 10^{-3}$ is highly intermittent and is characterized by discrete deposition bursts during which a seemingly random number of particles settle simultaneously on the bottom lid. These deposition bursts are separated by hiatuses, or plateaus, of random duration. Furthermore, as shown in figures 8(*b*) and 8(*c*), the resulting staircase-like curve exhibits self-similar structure at smaller scales when it is magnified up to the resolution of the number of particles and time step of the simulation. Therefore, the results shown in figure 8 point to the conclusion that the sedimentation curve for $v_s = 10^{-3}$ is the fractal object known as the devil's staircase curve (Bak 1986; Sotiropoulos *et al.* 2001). The devil's staircase has been found to emerge in a number of nonlinear systems, in both physics and engineering, undergoing a mode-locking transition to chaos. In such systems, the staircase has been shown to describe the dynamical behaviour as a function of frequency with the characteristic plateaus indicating locking at various rational frequencies (for specific examples, see Bak 1986; Lacis *et al.* 1997; Reichhardt & Nori 1999). Perhaps a more relevant and rather striking analogy with the physical phenomenon we consider in this work is the apparent emergence of devil's staircase distributions in stratigraphic records describing sediment accumulation in nature over geological time scales (Sadler 1981, 1999). This analogy will be discussed in more detail later on in this paper. What determines the emergence of the devil's staircase in the sedimentation process in the container flow appears to be the transition between the chaotic state, for which particles never settle but remain suspended and get stirred by the flow indefinitely, and the complete equilibrium state with all particles lying on the bottom lid. In this transitional fractal regime, which is obviously driven by the competition between inertia and gravitational forces, particles remain suspended during lapses of time, which correspond to the plateaus of the curve, followed by instantaneous sedimentation events within which groups of particles get deposited simultaneously on the bottom lid and never return to the flow.

It is important to point out that in this work we made no attempt to determine via numerical experiments the exact range of settling velocities within which the fractal sedimentation regime emerges. This is a computationally challenging task, since there are at least three governing parameters whose combination determines the emergence of the fractal regime: (i) the Reynolds number of the flow, (ii) the particle diameter (i.e. the Stokes number) and (iii) and the particle Froude number. Another parameter that could also be important in this regard is the specific gravity of the particles, which has been kept constant throughout this work. Exploring this multi-dimensional phase space via numerical simulations is a significant undertaking that will be left as

a topic for future research. Nevertheless, the results we reported in figure 8 along with several additional numerical experiments for various Reynolds numbers, which are not included for space considerations, do show conclusively that for a given Reynolds number there is a range of intermediate values of the settling velocity within which fractal sedimentation occurs.

It is also worth noting that the sedimentation times for each particle, all of which are embedded within the devil's staircase, are closely linked to the Lagrangian average maps presented in the previous section. To illustrate this connection, first note that the sedimentation time is essentially the stop time of the dynamical system consisting of the particle trajectory equations. Since particles start from a known initial position, the time that every particle takes to reach its respective stop time t_{stop} occurs when the centre of mass of the particle is located at a distance $d/2$ away from the bottom lid, which can be related to the Lagrangian average of the vertical velocity, $\bar{v}_3^L$, as follows:

$$x_3(t_{stop}) = \int_0^{t_{stop}} v_3(\boldsymbol{x}_0, \boldsymbol{x}, t)\ \mathrm{d}t = t_{stop}\,\bar{v}_3^L, \tag{5.1}$$

where $\boldsymbol{x}_0$ is the particle initial position; $x_3(t_{stop}) = d/2$ is the final vertical position of the particle when it reaches the bottom lid; and v_3 is the instantaneous particle velocity at position $\boldsymbol{x}$. Due to the increments in velocity when particles are in contact with the bottom lid (in our simulations particles that sediment are not removed but stay attached to and rotate with the bottom lid), the Lagrangian average maps shown in figures 6(c) and 6(d) for particles starting in the chaotic region of the flow exhibit a fractalized structure with patches of higher U^L. For 50 lid rotations, multiple small darker-colour regions emerge in the Lagrangian average map as seen in figure 6(c). These results are more evident in figures 6(e) and 6(f). Due to the larger settling velocity v_s, the sedimentation times t_{stop} are shorter, and few particles remain in suspension, which are represented by the lighter-colour patches non-uniformly distributed in the chaotic region.

To formally establish the fractal character of the curve shown in figure 8 we can count the spaces between plateaus that ultimately shrinks to the Cantor set associated with the devil's staircase construction. Following the methodology described by Bak (1986) and Sotiropoulos *et al.* (2001), we calculate the total width of plateaus that are larger than a time scale r, defined as $T(r)$. Subsequently we compute the space between steps, representing the time intervals when depositional events can be identified using a scale r: $T_{max} - T(r)$, where T_{max} is the total time of the computation. We then measure this quantity to obtain the total number of time windows $N(r)$ with magnitude r, required to contain all the segments previously calculated:

$$N(r) = \frac{T_{max} - T(r)}{r}. \tag{5.2}$$

For a devil's staircase curve, the variation of $N(r)$ should exhibit a power-law relation with the time scale r, such that

$$N(r) \sim (1/r)^{D_0}, \tag{5.3}$$

where D_0 is the fractal dimension of the Cantor set associated with the devil's staircase curve.

We apply the above algorithm to deposition curves obtained for successively larger particle ensembles (released along concentric circles covering the top lid), since, as has already been shown by Sotiropoulos *et al.* (2001), a converged fractal dimension is only obtained above a threshold particle ensemble size. Numerical sensitivity experiments showed that for $Re = 350$ and $Re = 700$, 2×10^4 particles are required

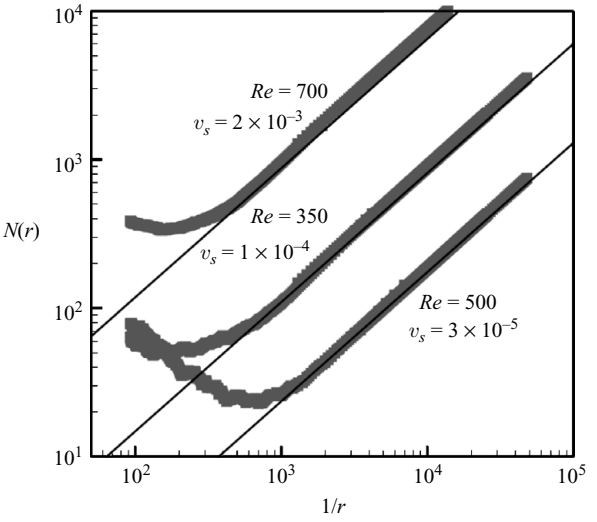

FIGURE 9. Fractal dimension of the devil's staircase for different Reynolds numbers. The symbols are the numerical results while the lines correspond to a slope of 0.87.

for converged solutions, while for $Re = 500$ twice as many particles are required for convergence. This apparent non-monotonic variation of the number of particles required for convergence with Reynolds numbers is due to the fact that as shown by Lackey & Sotiropoulos (2006) the stirring rate for this flow is maximized at $Re = 500$. The cases shown in figure 9 for the deposition of inertial particles are computed for three Reynolds numbers, with different numbers of total particles in each computation released in concentric circles from the top lid: 2×10^4 particles for $Re = 350$ and $Re = 700$ and 4×10^4 particles for $Re = 500$. As seen in figure 9, the departure from the power-law relationship occurs only at small $1/r$ corresponding to large plateaus that require long times of computation, when particles with long residence times inside the container settle. Since the last remaining particles can have arbitrarily long residence times, the integration time requires excessive computational resources for the large number of particles employed in the computation. Remarkably, for all cases the same value for the fractal dimension D_0 emerges. Namely we find $D_0 = 0.87$ which is essentially identical to the 'universal' value found in numerous dissipative dynamical systems in nature (Bak 1986).

It is important to note that Sotiropoulos *et al.* (2001) were the first to demonstrate that the devil's staircase emerged in chaotically advected flows. They observed the devil's staircase distribution for passive particles in the emptying of steady, three-dimensional vortex breakdown bubbles in a cylindrical container with a rotating bottom. Sotiropoulos *et al.* (2001) showed that for a range of swirl velocities, very small, steady three-dimensional perturbations of the Eulerian velocity field can give rise to very rich Lagrangian dynamics of passive tracers in the interior of vortex breakdown bubbles, characterized by KAM-tori cantori periodic islands and a large chaotic sea. Passive particles entering this dynamically rich region of the flow were shown to exit the vortex breakdown bubble via a series of random bursting events separated by hiatuses of random duration in a similar manner as the fractal sedimentation mechanism for inertial particles depicted in figure 8. Sotiropoulos *et al.* (2001) calculated the fractal dimension of the resulting devil's staircase distribution for various Reynolds numbers. They found values that depend on the Reynolds number

and are overall smaller than the 0.87 value we have found herein. This difference, however, should not be surprising, as the passive particles considered in the work of Sotiropoulos *et al.* (2001) comprise a volume-preserving dynamical system, whereas the inertial particles we have studied herein comprise a dissipative dynamical system. As already mentioned above, the 0.87 value appears to be 'universal' in a wide range of dissipative dynamical systems including the present case.

A remarkable phenomenon that is analogous to the process we uncovered herein is the emergence of the devil's staircase in sedimentary records observed over geological time scales. Through an exhaustive analysis of stratigraphic data Sadler (1981, 1999) was the first to observe that sedimentation processes in nature are characterized by unsteady and discontinuous events of deposition. Records of sediment accumulation over a range of time scales of several orders of magnitude yield staircase-like plots, containing hiatuses that correspond to periods of erosion or no deposition. Sadler (1981, 1999) applied scaling concepts to show that the variation of the rate of sediment accumulation is proportional to the time scale employed to measure it, finding power-law relations for the mean rate of sediment accumulation in time.

The fractal deposition of inertial particles observed in the present flows acquires great relevance in the context of Sadler's work. The results shown in figures 8 and 9 raise intriguing questions regarding the origin of the fractal accumulation rate in stratigraphic records and the possible role of chaotic advection in the transport and deposition of sediment in natural aquatic environments. Since chaotic advection is a fundamental mechanism of transport and stirring in geophysical flows, as shown for coastal regions (Ridderinkhof & Zimmerman 1992), further investigations are required to determine its relation to sediment transport and the intermittent accumulation of sedimentary deposits (Sadler 1981). Our results also emphasize the need to study geomorphologic systems coupling the flow and sediment dynamics. Chaotic dynamics may arise due to the complex interactions between the coastal and inland water flows and the earth's surface, leading to the alternation of random periods of stirring and transport with depositional episodes of sediment accumulation.

5.1. *Stirring rate of inertial particles*

In this section we seek to examine the effect of inertia on particle stirring relative to the passive particle case, which was studied in detail by Lackey and Sotiropoulos (2006). We quantify the stirring rates using the variance of concentration numerical technique developed by Lackey & Sotiropoulos (2006), which was based on the experimental analysis of Voth *et al.* (2003). The variance of concentration is a statistic employed to quantify the effectiveness of the flow in stirring the particles inside the container. Lackey & Sotiropoulos (2006) calculated the variance of concentration $\sigma_c^2(t)$ for passive particles by collapsing the azimuthal direction for every instant in time and then computing the instantaneous particle concentration at every grid node in a two-dimensional plane. As particle trajectories are stretched and folded inside the container, their distribution becomes more uniform in time, decreasing the magnitude of $\sigma_c^2(t)$ (see Lackey & Sotiropoulos 2006 for details). In the inertial particle case, if the settling velocity is large enough to produce sedimentation, particles can accumulate on the bottom lid and increase the variance of concentration magnitude in time, as will be subsequently shown.

A brief description of the technique of Lackey & Sotiropoulos (2006) is as follows. At every instant in time, the instantaneous three-dimensional particle positions are collapsed in the azimuthal θ direction, and the resulting two-dimensional plane is divided in control volumes that cover the entire domain and are associated with the

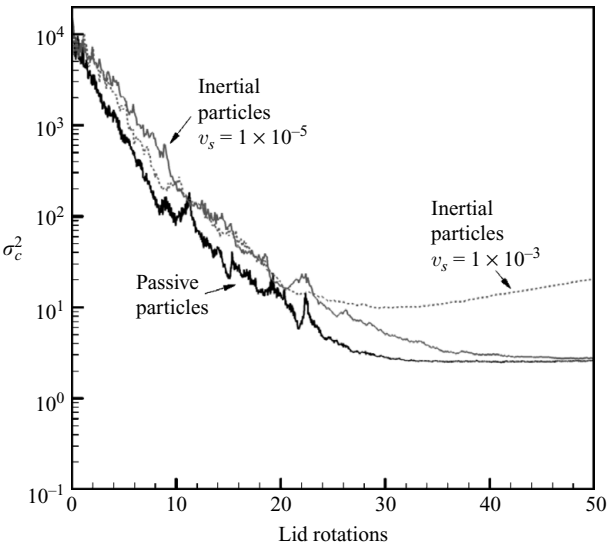

FIGURE 10. Variance of concentration at $Re = 500$ for inertial particles with $d = 0.002$ (grey and dashed lines) and for passive particles (black solid line), to quantify the decrease in the stirring rate due to inertia.

(i, j) nodes in the r–z space. By defining as n_{ij} the number of particles inside the control volume identified by the node (i, j) at time t, we compute the instantaneous discrete particle concentration as follows:

$$C_{ij}(t) = \frac{n_{ij}(t)}{N}, \tag{5.4}$$

where N is the total number of particles. The statistical variance of the discrete concentration field is therefore calculated at every instant in time as

$$\sigma_c^2(t) = \frac{1}{I \times J} \sum_{i}^{I} \sum_{j}^{J} \left[C_{ij}(t) - \bar{C}(t) \right]^2, \tag{5.5}$$

where I and J are the maximum number of grid nodes in the radial and vertical directions respectively, and the mean instantaneous concentration is computed as follows:

$$\bar{C}(t) = \frac{1}{I \times J} \sum_{i}^{I} \sum_{j}^{J} C_{ij}(t). \tag{5.6}$$

We compute $\sigma_c^2(t)$ for particles released along concentric circles on the top lid, simulating passive and inertial particles ($d = 0.002$, $v_s = 1 \times 10^{-5}$ and $v_s = 0.001$) at $Re = 500$ as shown in figure 10. Note that this specific Reynolds number is selected herein because according to the results of Lackey & Sotiropoulos (2006) this is the Reynolds number at which stirring rate is maximized for this flow. We use the same initial conditions in all the simulations for a total period of computation of 50 lid rotations, which was the appropiate time considered to mix passive particles in the container (Lackey & Sotiropoulos 2006).

The results shown in figure 10 clearly show that the decay of the variance is faster for both sets of passive particles, which leads to the important conclusion that particle inertia decreases the stirring rate. Lackey & Sotiropoulos (2006) quantified the stirring

rate of the flow as the rate at which $\sigma_c^2(t)$ decreases. They fitted an exponential decay curve to the calculated $\sigma_c^2(t)$ time series, such that the time evolution of the statistic can be expressed as

$$\sigma_c^2(t) = C_0 \ \exp(-R_m t) + C_1, \tag{5.7}$$

where C_0 and C_1 are constants.

By applying this technique to the results shown in figure 10, we find that the ratio of the stirring rates for inertial particles ($v_s = 1 \times 10^{-5}$) to those of passive particles is equal to $R_m^I / R_m^P = 0.88$. The reason for the slower stirring rate in this case is obviously due to the effects of inertia, which depending on the Stokes number can decelerate the stirring process.

The emergence of this phenomenon can be attributed to the accumulation or non-homogeneous spatial distribution of particles, also known as preferential concentration of inertial particles first observed by Squires & Eaton (1991) in turbulent flows. Using a model similar to the one employed in the present investigation to represent the dynamics of inertial particles, Bec (2005) also described the phenomenon of particle clustering or preferential concentration using scaling analysis for the spatial distribution of particles in two-dimensional and three-dimensional flows. He studied the particle trajectories neglecting gravity and other forces in the momentum equation, integrating the dynamics in simple random flows generated as sums of Fourier modes. The fractal characteristics of the inertial particle positions in two-dimensional and three-dimensional flows were described in terms of the Stokes numbers of the particles. Bec's simulations showed that clustering and reduced mixing occurred for small Stokes numbers, while for larger St particles occupied the entire space.

Therefore, these preliminary results for the variance of concentration not only demonstrate the differences between passive and inertial particles for the same statistics studied in detail by Lackey & Sotiropoulos (2006) but also pose important questions regarding the dependence of stirring rates on particle parameters. Further analyses, however, are required to establish the actual inertial effects on stirring rates and to determine the evidence of particle clustering in the flows inside the container. A systematic investigation of the dependence on the parameters that control stirring rates and the depositional regime described in the previous section will be reported in future communications.

Finally we should mention that for the particles with the highest settling velocity ($v_s = 0.001$) in figure 10, significant deposition occurs within the simulated time interval. For this reason the variance of concentration is seen to decay initially, but its magnitude increases slowly with time as particles start depositing and accumulating on the bottom lid.

6. Conclusions

We carried out simulations of the inertial particle dynamics in the three-dimensional flow in a cylindrical container with exactly counter-rotating lids. We described separately the motion of particles in the invariant and mixing regions of the flow in terms of different values of the non-dimensional particle diameters and Froude numbers, which can also be expressed collectively in terms of a non-dimensional settling velocity, to account for the effects of inertia and gravity, respectively. We have shown using Poincaré maps that for the range of studied parameters, the uniform flow field inside invariant regions constitute strong barriers to transport, trapping heavy particles for long periods of time as has been observed in previous

theoretical (McLaughlin 1988) and experimental investigations (Wereley *et al.* 2002; Abatan *et al.* 2006). Larger particle diameters, and in consequence larger Stokes numbers, set the conditions to increase stirring rates in these regions by allowing particles to escape.

The Lagrangian averaging technique (Mezić & Wiggins 1999; Mezić & Sotiropoulos 2002) was utilized to investigate the passive particle dynamics in the vicinity of the invariant toroidal regions in the flow. We identified for the first time a complex distribution of periodic orbits nested and folded near the tori boundaries. The same technique was applied to study inertial particle trajectories, demonstrating that invariant regions of the flow persist for inertial particles as well. Inside both the tori and the folded structures around them that contain periodic orbits, particles remain trapped for long periods of time, following closely the trajectories observed for passive particles for the simulated range of parameters.

Inertial particles are capable of remaining trapped in the tori and surrounding complex Lagrangian structures. However, inertial effects do have a profound impact on the extent of the invariant core and the structure of the dynamics in its vicinity. Small increments of the particle diameter were shown to reduce considerably the area occupied by the tori in the Lagrangian maps, and major changes can occur in the spatial distribution of the exterior islands that persist for all the simulations with large and small St.

For the range of parameters studied in this investigation, the Stokes number is critical to characterize the behaviour of particles in the toroidal invariant regions. On the other hand, the gravity term characterized by the Froude number only establishes the magnitude of the perturbation that can help the particles to escape. It is important to note that the parameter values were mainly selected to maintain a realistic range of St and Fr for the specific gravity and non-dimensional particle diameters chosen, such that the governing equations of the particles (3.6) and the one-way coupling assumptions remain valid.

Multiple aspects of the Lagrangian particle dynamics for the passive and inertial cases that we uncover in the present investigation will require further research, particularly the characteristics of the newly discovered flow regions that appear as intricate folds near the tori boundaries. Numerical and experimental studies might be needed to understand the flow dynamics in these regions and to parameterize their spatial distribution in terms of Re and AR and the diameter d and Fr in the inertial particle case.

In the chaotically advected region of the flow, the gravitational force has a preponderant role in the particle dynamics, overcoming inertia for small values of the Froude number leading to particle deposition. The competition between the inertial and gravity forces can produce a fractal sedimentation regime represented by the devil's staircase, with a fractal dimension very close to 0.87, which has also been found in other dissipative dynamical systems. The non-dimensional settling velocity defined in terms of St and Fr appears to be the relevant parameter defining the size of the phase-space window within which this striking fractal sedimentation regime emerges for a given Reynolds number.

The intermittent settling of particles observed in the fractal sedimentation process has also been shown to occur in other chaotically advected flows such as in the emptying process of steady vortex breakdown bubbles in confined flows (Sotiropoulos *et al.* 2001). In the case of vortex breakdown bubbles, however, the fractal emptying mechanism was observed for passive particles exiting from a chaotically advected sub-region of the flow (the interior of a perturbed vortex breakdown bubble). Furthermore,

for this case the fractal dimension of the devil's staircase was not 'universal' but was found to depend on the Reynolds number of the flow.

The effects of inertia on the stirring rate of the flow were quantified using the variance of concentration $\sigma_c^2(t)$, which was the same statistic employed by Lackey & Sotiropoulos (2006) to quantify the stirring rate of passive particles in the same flow. We computed $\sigma_c^2(t)$ for passive and inertial particles at $Re = 500$, which is the Reynolds number with the largest stirring rate for passive particles (Lackey & Sotiropoulos 2006). The stirring rate for inertial particles was found to be slower than the passive particle case. Further analyses are required to determine if this phenomenon can be attributed to the inhomogeneity produced by particle clustering due to inertia, as observed in unsteady random flows (Squires & Eaton 1991; Bec 2005).

Future research will also focus in the effects that chaotic advection can have on sediment transport and deposition in flows driven by slowly varying vortical structures, to determine the influence of the flow dynamics in sedimentation and depositional patterns in nature. Since large-scale two-dimensional flows driven by tides in coastal regions can experience stretching and folding of trajectories for passive particles (Ridderinkhof & Zimmerman 1992), future work will seek to connect these phenomena with the dynamics of inertial particles and sedimentary deposition in geophysical flows. Even though sedimentation is probably the result of multiple physical processes, the relation between chaotically advected flows and sedimentation processes in nature can shed further insights into the fractal characteristics of sediment accumulation observed by Sadler (1981, 1999) in stratigraphic records.

This work was supported by NSF grants EAR-0120914 (as part of the National Center for Earth-Surface Dynamics) and EAR-0738726. C. E. has also been partially supported by Fondecyt grant 11080032. Computational resources were provided by the University of Minnesota Supercomputing Institute. We thank the anonymous referee who pointed out equation (5.1) and the insightful connection between sedimentation times and Lagrangian average maps.

REFERENCES

Abatan, A. A., McCarthy, J. J. & Vargas, W. L. 2006 Particle migration in the rotating flow between co-axial disks. *AIChE J.* **52**, 2039–2045.

Aref, H. 1984 Stirring by chaotic advection. *J. Fluid Mech.* **143**, 1–21.

Auton, T. R., Hunt, J. C. R. & Prud'homme, M. 1988 The force exerted on a body in inviscid unsteady non-uniform rotational flow. *J. Fluid Mech.* **197**, 241–257.

Bak, P. 1986 The devil's staircase. *Phys. Today* **39**, 38–45.

Bec, J. 2005 Multifractal concentrations of inertial particles in smooth random flows. *J. Fluid Mech.* **528**, 255–277.

Crowe, C. T., Troutt, T. R. & Chung, J. N. 1998 *Multiphase Flows with Droplets and Particles*. CRC Press.

Dávila, J. & Hunt, J. C. R. 2001 Settling of small particles near vortices and in turbulence. *J. Fluid Mech.* **440**, 117–145.

Escauriaza, C. 2008 Three-dimensional unsteady modelling of clear-water scour in the vicinity of hydraulic structures: Lagrangian and Eulerian perspectives. PhD thesis, University of Minnesota, Minneapolis, MN.

King, G. P., Rowlands, G., Rudman, M. & Yannacopoulos, A. N. 2001 Predicting chaotic dispersion with Eulerian symmetry measures: wavy Taylor-vortex flow. *Phys. Fluids* **13**, 2522–2528.

Lacis, S., Barci, J. C., Cebers, A. & Perzynski, R. 1997 Frequency locking and devil's staircase for a two-dimensional ferrofluid droplet in an elliptically polarized rotating magnetic field. *Phys. Rev.* E **55**, 2640–2648.

Lackey, T. C. & Sotiropoulos, F. 2006 Relationship between stirring rate and Reynolds number in the chaotically advected steady flow in a container with exactly counter-rotating lids. *Phys. Fluids* **18**, 053601.

Mackay, R. S., Meiss, J. D. & Percival, I. C. 1984 Transport in Hamiltonian systems. *Physica* D **13**, 55–81.

Malhotra, N., Mezić, I. & Wiggins, S. 1998 Patchiness: a new diagnostic for Lagrangian trajectory analysis in time-dependent fluid flows. *Intl J. Bifur. Chaos* **8**, 1053–1093.

Maxey, M. R. 1987 The motion of small spherical particles in a cellular flow field. *Phys. Fluids* **30**, 1915–1928.

McLaughlin, J. B. 1988 Particle size effects on Lagrangian turbulence. *Phys. Fluids* **31**, 2544–2553.

Mezić, I. 2001 Chaotic advection in bounded Navier–Stokes flows. *J. Fluid Mech.* **431**, 347–370.

Mezić, I. & Sotiropoulos, F. 2002 Ergodic theory and experimental visualization of invariant sets in chaotically advected flows. *Phys. Fluids* **14**, 2235–2243.

Mezić, I. & Wiggins, S. 1999 A method for visualization of invariant sets of dynamical systems based on the ergodic partition. *Chaos* **9**, 213–218.

Nore, C., Tartar, M., Daube, O. & Tuckerman, L. S. 2004 Survey of instability thresholds of flow between exactly counter-rotating disks. *J. Fluid Mech.* **511**, 45–65.

Nore, C., Tuckerman, L. S., Daube, O. & Xin, S. 2003 The 1:2 mode interaction in exactly counter-rotating von Kármán swirling flow. *J. Fluid Mech.* **477**, 51–88.

Reichhardt, C. & Nori, F. 1999 Phase locking, devil's staircase, Farey trees, and Arnold tongues in driven vortex lattices with periodic pinning. *Phys. Rev. Lett.* **82**, 414–417.

Ridderinkhof, H. & Zimmerman, J. T. F. 1992 Chaotic stirring in a tidal system. *Science* **258**, 1107–1111.

Rudman, M. 1998 Mixing and particle dispersion in the wavy vortex regime of Taylor–Couette flow. *AIChE J.* **44**, 1015–1026.

Sadler, P. M. 1981 Sediment accumulation rates and the completeness of stratigraphic sections. *J. Geol.* **89**, 569–584.

Sadler, P. M. 1999 The influence of hiatuses on sediment accumulation rates. In *On the Determination of Sediment Accumulation Rates. GeoResearch Forum* (ed. P. Bruns & H. C. Hass), pp. 25–60. Trans Tech.

Saffman, P. G. 1965 The lift on a small sphere in a slow shear flow. *J. Fluid Mech.* **22**, 385–400.

Solomon, T. H. & Mezić, I. 2003 Uniform resonant chaotic mixing in fluid flows. *Nature* **425**, 376–380.

Sotiropoulos, F., Ventikos, Y. & Lackey, T. C. 2001 Chaotic advection in three-dimensional stationary vortex-breakdown bubbles: Šil'nikov's chaos and the devil's staircase. *J. Fluid Mech.* **444**, 257–297.

Sotiropoulos, F., Webster, D. R. & Lackey, T. C. 2002 Experiments on Lagrangian transport in steady vortex-breakdown bubbles in a confined swirling flow. *J. Fluid Mech.* **466**, 215–248.

Squires, K. & Eaton, J. 1991 Preferential concentration of particles by turbulence. *Phys. Fluids* A **3**, 1169–1178.

Squires, T. M. & Quake, S. R. 2005 Microfluidics: fluid physics at the nanoliter scale. *Rev. Mod. Phys.* **77**, 977–1026.

Stommel, H. 1949 Trajectories of small bodies sinking slowly through convection cells. *J. Mar. Res.* **8**, 24–29.

Tsega, Y., Michaelides, E. E. & Eschenazi, E. V. 2001 Particle dynamics and mixing in the frequency driven Kelvin cat eyes flow. *Chaos* **11**, 351–358.

Tuval, I., Mezić, I., Bottausci, F., Zhang, Y. T., MacDonald, N. C. & Piro, O. 2005 Control of particles in microelectrode devices. *Phys. Rev. Lett.* **95**, 236002.

Voth, G. A., Saint, T. C., Dobler, G. & Gollub, J. P. 2003 Mixing rates and symmetry breaking in two-dimensional chaotic flow. *Phys. Fluids* **15**, 2560–2566.

Wang, L. P., Burton, T. D. & Stock, D. E. 1990 Chaotic dynamics of heavy particle dispersion: fractal dimension versus dispersion coefficients. *Phys. Fluids* A **2**, 1305–1308.

Wang, L. P., Burton, T. D. & Stock, D. E. 1991 Quantification of chaotic dynamics for heavy particle dispersion in ABC flow. *Phys. Fluids* A **3**, 1073–1080.

Wang, L. P., Maxey, M. R., Burton, T. D. & Stock, D. E. 1992 Chaotic dynamics of particle dispersion in fluids. *Phys. Fluids* A **4**, 1789–1804.

Wereley, S. T., Akonur, A. & Lueptow, R. M. 2002 Particle-fluid velocities and fouling in rotating filtration of a suspension. *J. Membr. Sci.* **209**, 469–484.

Wereley, S. T. & Lueptow, R. M. 1999 Inertial particle motion in a Taylor Couette rotating filter. *Phys. Fluids* **11**, 325–333.

Wiggins, S. & Ottino, J. M. 2004 Foundations of chaotic mixing. *Phil. Trans. R. Soc. Lond.* A **362**, 937–970.